JOURNAL OF AIRCRAFT
Vol. 30, No. 1, Jan.–Feb. 1993

Aeroelastic Tailoring Analysis for Preliminary Design of Advanced Propellers with Composite Blades

Takashi Yamane*
Mechanical Engineering Laboratory, Namiki, Tsukuba 305 Japan
and
Peretz P. Friedmann†
University of California, Los Angeles, California 90024

An analytical study of aeroelastic tailoring has been conducted to determine the flutter characteristics of advanced turbo propellers for preliminary design purposes. The structural dynamic model for composite propeller blades is combined with an unsteady cascade theory with three-dimensional corrections to produce an aeroelastic analysis tool for pretwisted propeller blades with homogeneous anisotropy exposed to a high subsonic flow. The free-vibration analysis of the SR-3 propeller model built of unidirectional graphite/epoxy, revealed that the first-bending frequency of the blade can be changed by 53% from the baseline value by changing fiber orientation. Using *p-k* modal flutter analysis it was also found that the fiber orientation with a little larger sweep angle than that of the elastic axis can eliminate flutter without any weight penalty, and that the corresponding first natural mode has the least bending-torsion coupling. However, the flutter velocity is sensitive to fiber orientation and interblade-phase angle.

Nomenclature

$[A_R]$, $[A_I]$ = real and imaginary parts of aerodynamic stiffness matrix
a = nondimensional axial-induced velocity
B = number of blades
b = nondimensional angular-induced velocity
C' = equivalent unsteady lift-deficiency function, $C'(k) = (-W/\pi\dot{h})(L/\rho cW^2) - (ik/2)$, where L is unsteady lift
$[C_{ij}]$ = material stiffness matrix
C_L = section-lift coefficient
c = chord length normal to the pitch-change axis
$[D]$ = system damping matrix
F = Prandtl's finite-span correction factor, Eq. (12)
$\{F_T\}$ = generalized forces composed of aerodynamic forces and steady centrifugal forces
h = leading-edge heave, normal to the helical wake surface, positive up
$[J]$ = Jacobian matrix for the Newton-Raphson method
$[K_L]$, $[K_{NL}]$ = linear and nonlinear stiffness matrices
k = reduced frequency at the reference section, $\omega c/2W$
$[M]$ = system mass matrix
M_0 = helical Mach number, W/(sound velocity)
p = Laplace operator in the p-k analysis
Δp = pressure perturbation
$[Q_{ij}]$ = condensed material stiffness matrix
$\boldsymbol{q}$ = general coordinate vector of the beam, Eq. (10)
R = rotor radius
r = radius from the center of rotation
$[S_{ij}]$ = material compliance matrix, $[C_{ij}]^{-1}$
s = blade spacing, namely leading-edge distance
$[T]$ = transformation matrix for size reduction
t = time
u, v, w = radial, lead, and flap displacements of the shear center
Δu, Δv = axial and tangential velocity perturbations
V = axial velocity
W = resultant velocity at the cascade
w = velocity normal to the chord
x, y = orthogonal coordinates of the cascade
x, η, ζ = curvilinear coordinates of the beam
x_{SC} = shear-center distance from the area centroid, positive aft
z, z_0 = coordinates along chord, origin is the leading edge
α_r, β_r = rth wave numbers in the x and y directions
β = blade pretwist angle, measured from the pitch angle at 75% radius
$\beta_{0.75}$ = blade pitch angle at 75% radius, measured from the plane of rotation
Γ_i' = amplitude of circulation per unit chord, being subtracted the free vortex component
δ = section pitch angle around the leading edge, positive trailing edge up
ε_{xx}, $\gamma_{x\eta}$, $\gamma_{x\zeta}$ = normal, shear, and shear strain components
θ_s = stagger angle, namely angle between resultant velocity and axial velocity
Λ = aerodynamic sweep angle, positive sweep back
Λ_F = fiber sweep angle from the pitch change axis
λ = local speed ratio, $r\Omega/V$
ρ = air density
σ = interblade-phase angle
τ = chordwise distribution of the airfoil semithickness
$[\Phi_2]$, $[\Phi_3]$ = quadratic and cubic Hermite interpolation polynomials
ϕ = elastic twist angle, positive leading-edge up
Ψ = Saint-Venant torsion-type warping function, positive convex
Ω = angular velocity of the rotor
ω = system frequency
$(\,)^{(i)}$ = value of the ith iteration

Presented as Paper 90-1160 at the AIAA 31st Structures, Structural Dynamics and Materials Conference, Long Beach, CA, April 2–4, 1990; received Aug. 2, 1990; revision received Nov. 15, 1991; accepted for publication Dec. 26, 1991.

*Senior Researcher, Energy Engineering Department.
†Professor, Mechanical, Aerospace and Nuclear Engineering Department. Fellow AIAA.

$( )r$ = value of the rth cascade wave
$[ ]^T$ = transpose
$( ), x$ = partial derivative with respect to x

Introduction

THE advanced turbo propellers (ATP) represent a new propulsion system which maintains high efficiency, at high speeds similar to that of conventional turboprop engines, at cruising speeds similar to that in turbofan engines. Characteristics of the ATP blades are 1) high-sweep angles to reduce the effective Mach number; 2) low-aspect ratio to generate high power with a limited size; and 3) low-thickness ratio to reduce noise and drag.

Wind-tunnel experiments done by Mehmed et al.[1,2] revealed that the ATP blades can encounter bending-torsion flutter. The importance of cascade effects was also noted. To improve flutter characteristics of the ATP, several ideas such as aeroelastic tailoring,[3,4] blade mistuning,[5] mass balance,[4] and geometry modification[4] have been examined.

One of these ideas, the aeroelastic tailoring technique which utilizes the anisotropy of composites, has the potential for eliminating flutter from the ATP without any weight penalties. Though several experiments indicated the validity of the technique,[3,4] a fairly simple analysis, useful for preliminary design purposes, is not available at present.

Attempts at sophisticated flutter analyses can be found in Refs. 6 and 7. The purpose of our article is to provide a fairly simple analysis tool for the preliminary design of the ATP blades which can be useful for trend studies aimed at determining the effectiveness of aeroelastic tailoring for the ATP.

In this article, the structural dynamic model for composite pretwisted propeller blades with homogeneous anisotropy is combined with an unsteady compressible cascade model to produce an aeroelastic analysis tool. The blade is modeled as a set of rotating beam elements with pretwist, moderate deflections, and section warping based on the model developed by Kosmatka and Friedmann[8,9] for general anisotropic materials. For unsteady aerodynamic analysis, unsteady compressible cascade theory developed by Smith[10] is combined with the sweep and finite-span corrections based on modified strip theory. The present analysis is aimed at including, e.g., the compressibility correction at Mach number up to 0.8, the cascade effect of an 8- to 10-bladed rotor, the effect of sweep up to 45 deg, and the finite-span effect due to span-chord ratio less than 5.

By applying the present analysis to the SR-3 propeller model made of unidirectional graphite/epoxy, the effects of fiber orientation on flutter velocities and the corresponding natural modes and frequencies are examined. The effects of interblade-phase angle as a cascade are also examined. Finally basic aeroelastic tailoring will be used to eliminate flutter.

Structural Dynamic Analysis

Rotating Anisotropic Beams with Pretwist and Sweep

The ATP blades can be regarded as rotating anisotropic beams with pretwist and sweep. Kosmatka and Friedmann[8,9] derived the following curvilinear strain expressions in terms of shear center displacements in a Cartesian coordinate system defined for each element (u, v, w, ϕ), and section curvilinear coordinates (x, η, ζ):

$$\begin{aligned}
\varepsilon_{xx} &= u_{,x} + (v_{,x}^2 + w_{,x}^2)/2 + (\phi_{,x}^2/2 + \beta_{,x}\phi_{,x})(\eta^2 + \zeta^2) \\
&\quad + (\Psi\phi_{,x})_{,x} - v_{,xx}\{\eta\cos(\beta + \phi) - \zeta\sin(\beta + \phi)\} \\
&\quad - w_{,xx}\{\zeta\cos(\beta + \phi) + \eta\sin(\beta + \phi)\} \\
\gamma_{x\eta} &= (\Psi_{,\eta} - \zeta)(\phi_{,x} + \phi_0) \\
\gamma_{x\zeta} &= (\Psi_{,\zeta} + \eta)(\phi_{,x} + \phi_0) \\
\phi_0 &= \{w_{,x}\cos\beta - v_{,x}\sin\beta\}\{v_{,xx}\cos\beta + w_{,xx}\sin\beta\}
\end{aligned} \tag{1}$$

where u is taken along the elastic axis, v is taken in the plane determined by the elastic axis and the chord at 75% radius, and w is taken normal to the plane as shown in Fig. 1. The curvilinear coordinate system (x, η, ζ) rotates about the elastic axis by the amount of pretwist, $\beta(x)$. The total system equations of motion can be obtained from the discretized Hamilton's principle for n elements

$$\int_{t_1}^{t_2} \sum_{e=1}^{n} (\delta U - \delta T - \delta W_E)\, dt = 0 \tag{2}$$

where U, T, and W_E denote strain energy, kinetic energy, and work done by nonconservative forces, respectively. The above equation implies that the total dynamic potential, $\Sigma_e(U - T - W_E)$, is an extremum over the time integral from t_1 to t_2. The variation of strain energy can be obtained by

$$\delta U = \int_V \begin{Bmatrix} \delta\varepsilon_{xx} \\ \delta\gamma_{x\zeta} \\ \delta\gamma_{x\eta} \end{Bmatrix}^T \begin{bmatrix} Q_{11} & Q_{15} & Q_{16} \\ Q_{15} & Q_{55} & Q_{56} \\ Q_{16} & Q_{56} & Q_{66} \end{bmatrix} \begin{Bmatrix} \varepsilon_{xx} \\ \gamma_{x\zeta} \\ \gamma_{x\eta} \end{Bmatrix} dV \tag{3}$$

where $[Q_{ij}]$ reflects anisotropy of the material and is condensed from the 6×6 stiffness matrix $[C_{ij}]$ based on the assumption for stresses as follows:

$$\sigma_{\eta\eta} = \sigma_{\zeta\zeta} = \tau_{\eta\zeta} = 0 \tag{4}$$

The matrix $[C_{ij}]$ can be obtained through rotation of the stiffness matrix,[11] expressed in terms of nine independent elastic constants in the case of an orthotropic material, by the differential angle between the fiber orientation and the elastic axis orientation. The variation of kinetic energy δT is described in terms of shear-center displacements, section warping, and curvilinear coordinates. The virtual work δW_E is composed of steady and unsteady aerodynamic forces. The complete expressions for δU, δT, and δW_E, with the exception of the aerodynamic loads, are given in Ref. 9.

In the case of a cross section which resembles an ellipse $(\eta^2/a^2 + \zeta^2/b^2 = 1)$ and has a homogeneous anisotropy, Saint-Venant torsion-type warping function is given by[13]

$$\Psi(\eta, \zeta) = \frac{S_{45}a^2}{S_{44}b^2 + S_{55}a^2}\left(\zeta^2 - \frac{b^2\eta^2}{a^2}\right) + \frac{S_{44}b^2 - S_{55}a^2}{S_{44}b^2 + S_{55}a^2}\cdot\eta\zeta \tag{5}$$

where $[S_{ij}] = [C_{ij}]^{-1}$ is a compliance matrix. In the case of a thin airfoil section with homogeneous anisotropy, an approx-

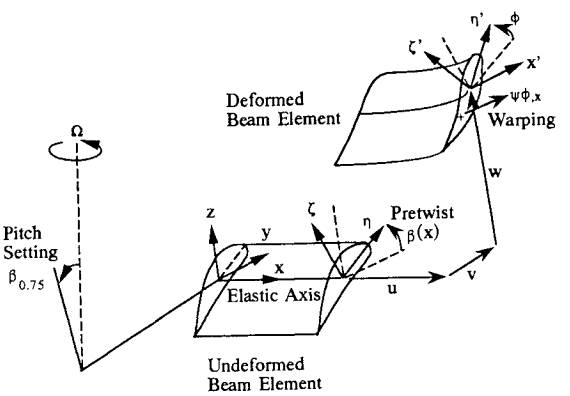

Fig. 1 Coordinate systems.

imate equation for the shear-center location can be derived through a slight modification to Ref. 13 as follows:

$$x_{SC} = \left[\left(1 - \frac{4S_{13}}{S_{55}}\right)\int_{LE}^{TE} \tau^3 x\, dx - \left(\frac{3}{4}\frac{S_{36} + S_{45}}{S_{55}}\right) \cdot \int_{LE}^{TE} \tau^4\, dx\right] \cdot \left(\int_{LE}^{TE} \tau^3\, dx\right)^{-1} \quad (6)$$

where the section contour is assumed as $y = \pm\tau(x)$, and $x = 0$, LE, and TE corresponds to the section area centroid, the leading edge, and the trailing edge, respectively. More accurate values of the warping function and the shear-center location of arbitrarily laminated composite cross sections can be obtained from the analysis described in Refs. 9 and 12.

Finite-Element Analysis

The shear-center displacements are described by Hermite interpolation polynomials within jth beam element as follows:

$$\begin{aligned} v &= \{\Phi_3(x)\}\{v^{j-1},\ v_{,x}^{j-1},\ v^{j},\ v_{,x}^{j}\}^T \\ w &= \{\Phi_3(x)\}\{w^{j-1},\ w_{,x}^{j-1},\ w^{j},\ w_{,x}^{j}\}^T \\ \phi &= \{\Phi_2(x)\}\{\phi^{j-1},\ \phi^{j},\ \phi^{j-0.5}\}^T \\ u &= \{\Phi_2(x)\}\{u^{j-1},\ u^{j},\ u^{j-0.5}\}^T \end{aligned} \quad (7)$$

where $\{\Phi_2(x)\}$ and $\{\Phi_3(x)\}$ denote a set of quadratic and cubic Hermite interpolation polynomials, respectively, and $(\ )^{j-0.5}$ implies midelement value. The following boundary condition is applied at the root cutoff:

$$\{v^0,\ v_{,x}^0,\ w^0,\ w_{,x}^0,\ \phi^0,\ u^0\} = \{0\} \quad (8)$$

The generalized equations of motion for $8n$ DOF are obtained as follows:

$$[M]\boldsymbol{q}_{,tt} + [D]\boldsymbol{q}_{,t} + [K_L + K_{NL}(\boldsymbol{q})]\boldsymbol{q} + \{F_T\} = \{0\} \quad (9)$$

where

$$\boldsymbol{q} = \{\phi^{0.5},\ u^{0.5};\ v^1,\ v_{,x}^1,\ w^1,\ w_{,x}^1,\ \phi^1,\ u^1;\ \ldots,\ \phi^n,\ u^n\}^T \quad (10)$$

The matrix $[K_{NL}]$ represents nonlinear stiffness due to moderate deflections, warping, and steady load effects, and $\{F_T\}$ refers to steady and unsteady aerodynamic forces as well as steady centrifugal forces.

Aerodynamic Analysis

Steady Momentum Analysis

Steady aerodynamic loads are calculated using Glauert's general momentum theory[14] including axial and angular momentum in combination with Prandtl's finite-span correction.[14] Where the axial-induced velocity and the angular-induced velocity at the disk plane are denoted by aV and $br\Omega$, respectively; they can be determined by

$$4Fa(1 + a) = \frac{Bc}{2\pi r} C_L\lambda(1 - b)[(1 + a)^2 + \lambda^2(1 - b)^2]^{1/2}$$

$$4F\lambda b = \frac{Bc}{2\pi r} C_L[(1 + a)^2 + \lambda^2(1 - b)^2]^{1/2} \quad (11)$$

$$C_L = \frac{C_{L\alpha}\cos\Lambda}{\sqrt{1 - M_0^2\cos^2\Lambda}}\left[\beta(r) + \beta_{0.75} - \tan^{-1}\frac{1 + a}{\lambda(1 - b)}\right]$$

The quantity F is Prandtl's finite-span correction factor; which for a B-bladed rotor is given by

$$F(a, b, r) = \frac{2}{\pi}\cos^{-1}\exp\left[\frac{B}{2}\left(\frac{r}{R} - 1\right) \cdot \left\{1 + \left(\frac{\lambda(1 - b)}{1 + a}\right)^2\right\}^{1/2}\right] \quad (12)$$

Finally, the steady blade section load can be obtained using the induced velocities a and b. The finite-span correction factor F is also used for the unsteady aerodynamic loads.

Unsteady Subsonic Cascade Analysis

Smith's unsteady subsonic cascade theory[10] is used combined with sweep and finite span corrections based on modified strip theory. A brief description of this methodology is provided next.

The cascade airfoil geometry is specified by chord length c, stagger angle θ_s, and blade spacing s. The pressure and two velocity components are expanded in Fourier series

$$\begin{Bmatrix}\Delta p\\ \Delta u\\ \Delta v\end{Bmatrix} = \sum_{r=-\infty}^{\infty}\begin{Bmatrix}p_r\\ u_r\\ v_r\end{Bmatrix}\exp i(\omega t + \alpha_r x + \beta_r y) \quad (13)$$

where x and y are the orthogonal coordinates in the directions of the axial flow and the tangential flow, respectively. Each velocity and pressure field is called a cascade wave which corresponds to a fundamental solution for isentropic inviscid flow. Since the cascade airfoils are regarded, a system where cascade waves are superposed. The normal induced velocity on the reference airfoil w can be determined by summing up all the cascade waves and integrating over the chord

$$\begin{aligned} w(z, t) &= \int_0^c \sum_{r=-\infty}^{\infty}\sum_{k=1}^{3} w^{(k)}\Gamma'\, dz \exp i(\omega t + \alpha_r x + \beta_r y)^{(k)} \\ &= \exp(i\omega t)\int_0^c \Gamma'(z_0)K\left(\frac{z - z_0}{c}\right)\frac{dz_0}{c} \end{aligned} \quad (14)$$

where Γ' is unit-chord circulation amplitude when the free vortex component is being subtracted, and K is a kernel function,[10] whose singularity can be removed by the method described in Ref. 10.

The boundary conditions are expressed in terms of leading-edge heave h and pitching δ as follows:

$$\frac{w}{W} = 2ik\left(\frac{h}{c} + \delta\frac{z}{c}\right) + \delta; \qquad k = \frac{\omega c}{2W} \quad (15)$$

where W denotes the resultant velocity and k is the reduced frequency. In the case of a propeller, h is defined as the elastic displacement normal to the helical stream lines, and δ is defined as the elastic twist angle about the radius. The structural variables which are defined along the line of shear centers will be transformed to these variables. The phase of airfoil motion have been assumed as

$$\exp i(\omega t + m\sigma); \qquad m = 0, \pm1, \pm2, \ldots, \pm\infty$$

where σ is called interblade-phase angle. Finally, the two-dimensional lift and moment about leading edge is obtained by integrating Γ' along the chord. This yields

$$\begin{aligned} L &= L_h(k, \sigma)h + L_\delta(k, \sigma)\delta \\ M &= M_h(k, \sigma)h + M_\delta(k, \sigma)\delta \end{aligned} \quad (16)$$

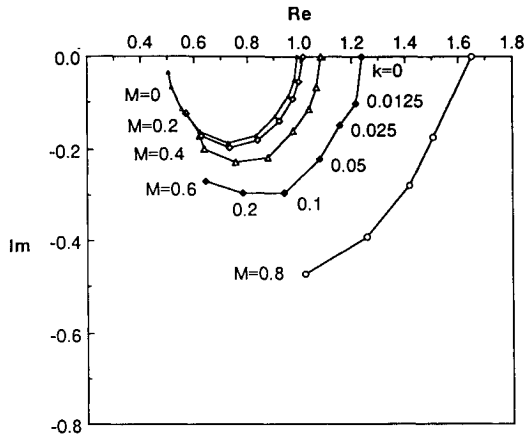

Fig. 2 Compressibility effect on equivalent unsteady lift deficiency function, $C'(k)$ ($\sigma = 0$, $\theta_s = 0$ deg, $s/c = 200$).

where the values of L_h, L_δ, M_h, M_δ are complex, and k is represented by the reduced frequency of a reference section. Reduced frequency for the jth element is given by $k_j = k(Wc_j/cW_j)$. Compressibility effects on the complex value of L_h is presented in Fig. 2 for the case of an isolated airfoil. The equivalent-lift deficiency function shown in Fig. 2 is the unsteady-to-steady lift ratio excluding the virtual mass term. Since the virtual mass term cannot be separated in compressible flow cases, it is denoted as "equivalent." In the calculation, the quantities

$$\gamma_i = \frac{\Gamma_i'}{W} \frac{\sin \psi_i}{2} \Delta\psi_i \tag{17}$$

where

$$\cos \psi_i = 1 - \frac{2z_0}{c}; \qquad i = 1, 2, \ldots, N$$

have been selected as unknown variables because they have a finite value at the leading edge. It can be shown that the computation time is almost proportional to the following index:

$$\frac{\text{Blade spacing}}{\text{Chord length}} \frac{[\text{Chordwise segment number}]^2}{\text{COSINE (Stagger angle)}} \tag{18}$$

Finite-Span and Sweep Correction

In order to account for three-dimensional finite-span effects, the two-dimensional unsteady subsonic aerodynamic loads should be multiplied by the finite-span correction factor F, which is identical to that used in the steady aerodynamic analysis. This can be regarded the simplest modified strip theory.[15]

On the other hand, when sweep angle at the quarter-chord is denoted by Λ and the effect of spanwise flow is neglected, the sweep correction for airfoils specified along the stream lines can be obtained by multiplying by cos Λ, the two-dimensional lift, and moment.[16] Furthermore, the effective Mach number is reduced to $M = M_0 \cos \Lambda$, where M_0 is helical Mach number. Furthermore, it is assumed that the drag per unit span is not affected by sweep angle. Finally the lift, drag, and moment per unit span can be obtained as follows[16]:

$$\begin{aligned} L_{3D} &= F \cos \Lambda L_{2D}(M = M_0 \cos \Lambda) \\ D_{3D} &= D_{2D} \\ M_{3D} &= F \cos \Lambda M_{2D}(M = M_0 \cos \Lambda) \end{aligned} \tag{19}$$

Modal Flutter Analysis

Steady Deformation

The steady blade deformations due to steady aerodynamic loads and centrifugal forces are determined first, by using the static part of Eqs. (9) given by

$$[K_L + K_{NL}(\boldsymbol{q})]\boldsymbol{q} + \{F_T(\boldsymbol{q})\} = \{0\} \tag{20}$$

The equilibrium position for $\boldsymbol{q}$ is obtained using the Newton-Raphson method. The general coordinates for the $(i + 0.5)$th iteration, $\boldsymbol{q}^{(i+0.5)}$, can be obtained by the following formula[9]:

$$\boldsymbol{q}^{(i+0.5)} = \boldsymbol{q}^{(i)} - [J^{(i)}]^{-1}\{[K_L + K_{NL}^{(i)}]\boldsymbol{q}^{(i)} + F_T^{(i)}\} \tag{21}$$

where

$$[J^{(i)}] = \{\partial/\partial \boldsymbol{q}^{(i)}\}\{[K_L + K_{NL}^{(i)}]\boldsymbol{q}^{(i)} + F_T^{(i)}\} \tag{22}$$

The reason for a noninteger superscript is explained next.

The converged nonlinear solution has to be generated carefully to avoid spurious solutions. Therefore, the following calculation scheme was adopted:

1) The rotational velocity is increased in small steps to avoid convergence to incorrect equilibrium positions. A converged solution in the previous step is used as the first approximation for the next step.

2) Both the line-search method as well as the Newton-Raphson (N-R) method are used since predictions given by the N-R method diverge rapidly when convergence is not achieved. As shown in Fig. 3, the line-search method calculates, in the $8n$-dimensional space, the residuals at several points along the line between the point of the previous step $\boldsymbol{q}^{(i)}$, and the newly predicted point by the N-R method $\boldsymbol{q}^{(i+0.5)}$. Specifically the residual evaluation points are given by the following relations:

$$\boldsymbol{q}^{(i,j)} = \left(1 - \frac{j}{J}\right)\boldsymbol{q}^{(i)} + \frac{j}{J}\boldsymbol{q}^{(i+0.5)}; \qquad j = 0, \ldots, J$$

where in the actual calculations the value of $J = 4$. The residual can be defined as the vector norm of the left side of Eq. (20). Then the method selects the minimum residual point as the approximation for the next step $\boldsymbol{q}^{(i+1)}$ from the various evaluation points, and the value $\boldsymbol{q}^{(i+0.5)}$ is deleted.

Modal Representation

After the nonlinear equilibrium position is obtained, linearization of Eq. (9) about the static equilibrium leads to

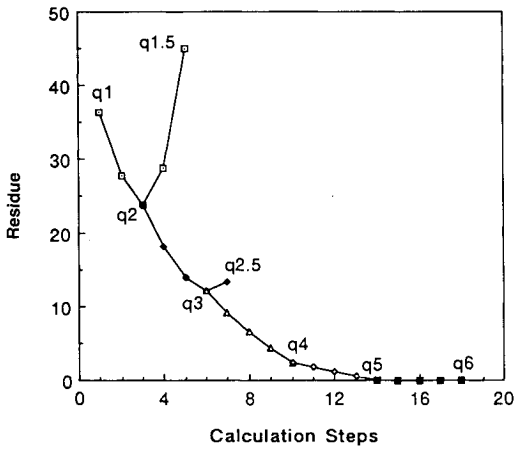

Fig. 3 Convergence example for the Newton-Raphson method combined with the line-search method.

the following equations:

$$[M]\ddot{q} + [D]\dot{q} + [K_L + K'_{NL}(q_0)]q + [A_R(k, \sigma) + iA_I(k, \sigma)]q = \{0\} \quad (23)$$

where the dimension of matrices is $8n \times 8n$ (n: number of elements) and $[K'_{NL}]$ is a linearized matrix of $[K_{NL}]$. A normal mode transformation is used because it reduces the size of the problem and it is also useful in identifying the flutter mode. When a transformation $q = [T]y$ is introduced where $[T]$ consists of the first m eigenvectors for the undamped system for each rotational velocity, the above $8n \times 8n$ system will be reduced to an $m \times m$ system

$$[m]\ddot{y} + [\mathrm{d}]\dot{y} + [k_{NL}]y + [a_R + ia_I]y = \{0\} \quad (24)$$

where

$$[m] = [T]^T[M][T]$$
$$[\mathrm{d}] = [T]^T[D][T]$$
$$[k_{NL}] = [T]^T[K_L + K'_{NL}][T]$$
$$[a_R + ia_I] = [T]^T[A_R + iA_I][T]$$

These equations give correct eigenvalues for the undamped system and a good approximation for weakly damped systems. The eigenvectors for transformation $[T]$ are obtained by a QZ type of eigenvalue analysis.

p-k Method

The aerodynamic matrices $[A_R + iA_I]$ or $[a_R + ia_I]$ are based on a simple harmonic motion; however, they give a good approximation for weakly damped systems at other points despite the fact that simple harmonic motion is achieved only at the flutter points. In this sense, the Laplace operator $p = \lambda + i\omega$, and Fourier operator $k = c\omega/2W$ (physically, reduced frequency at the reference section as was mentioned previously), are used simultaneously in the p-k method. Since p tends to $i\omega = i2kW/c$ near flutter points, imaginary unit $i = \sqrt{-1}$ may be approximated by $i \cong pc/2kW$. Therefore, the following eigenvalue problem with real matrices can be solved iteratively[17,18]

$$\left(\begin{bmatrix} k' & \mathrm{d}' \\ 0 & I \end{bmatrix} - p\begin{bmatrix} 0 & -m \\ I & 0 \end{bmatrix}\right)\begin{Bmatrix} y \\ \dot{y} \end{Bmatrix} = \begin{Bmatrix} 0 \\ 0 \end{Bmatrix} \quad (25)$$

where

$$[\mathrm{d}'] = [\mathrm{d}] + \frac{c}{2kW}[a_I(k, \sigma)]$$
$$[k'] = [k_{NL}] + [a_R(k, \sigma)]$$

until the reduced frequency converges to $k \cong Im(p)c/2W$ of the mode of interest. The above equations are exact for flutter points but give an approximation for other points.

Results and Discussion

Discretization by a Finite Element Model

The propeller model examined here is the SR-3 (described in Ref. 19) made of high-strength graphite/epoxy. The blade has pretwist angle of 31.2 deg from root to tip and a maximum aerodynamic sweep angle of 46.0 deg. The NACA 16 series is used as cross-sectional airfoils.

The three-dimensional line of shear centers, or the elastic axis, was determined first. The line through shear centers of the initial section profiles, which were defined perpendicular to the pitch-change axis, was taken as the first approximation. The nodal sections were replaced by those perpendicular to the approximate line of shear centers, and therefore, the elastic axis was obtained after a few iterations. The elastic-axis geometry and the finite-element grid for the structural dynamic analysis are shown in Fig. 4a. On the other hand, the grid for the aerodynamic analysis is shown in Fig. 4b. The aerodynamic grid differs from the structural dynamic grid, as expained below.

For the structural dynamic grid, the nodal sections should be perpendicular to the elastic axis based on the definition of the curvilinear coordinates used in each element. An exception is the tip section which has to coincide with the actual tip. This is because the mass property of the tip element has a major effect on the system characteristics, whereas precise structural modeling at the tip is less important.

For the aerodynamic grid, the nodal sections should have the same radius or, approximately, should be perpendicular to the pitch-change axis because the total pressure should be constant along each chord. Otherwise, two-dimensional aerodynamic theory cannot be used.

In the calculation when the structural dynamic grid is generated, the nodal points on the elastic axis are kept identical to those of the aerodynamic grid.

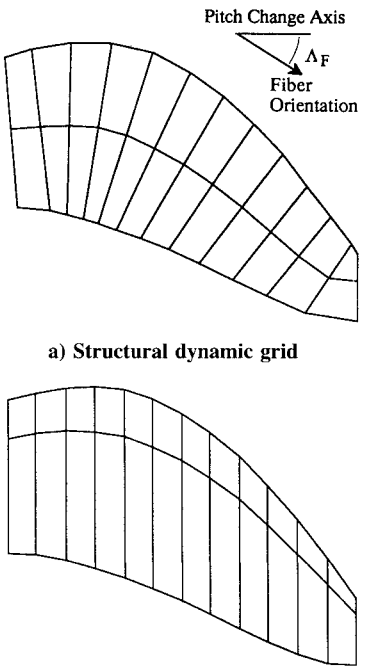

a) Structural dynamic grid

b) Aerodynamic grid

Fig. 4 Numerical grids for aeroelastic analysis (SR-3 propeller model made of unidirectional graphite/epoxy, pretwist angle = 31.2 deg).

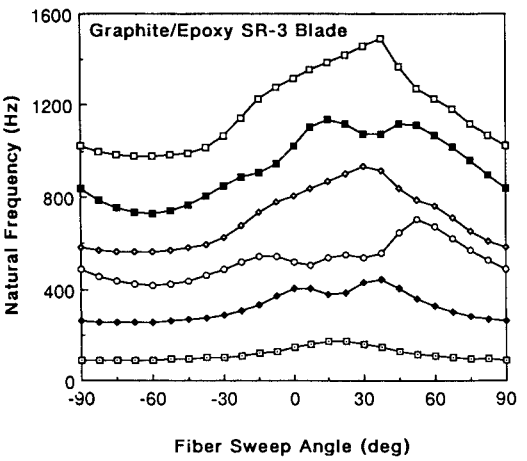

Fig. 5 Effect of fiber orientation on natural frequencies (SR-3 blade made of unidirectional graphite/epoxy).

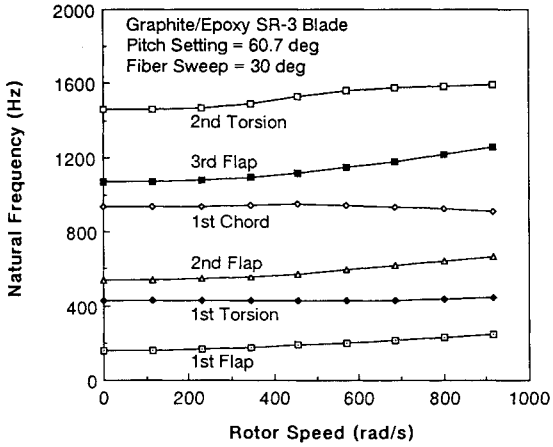

Fig. 6 Campbell diagram for a composite blade (graphite/epoxy, fiber sweep = 30 deg, $\beta_{0.75}$ = 60.7 deg).

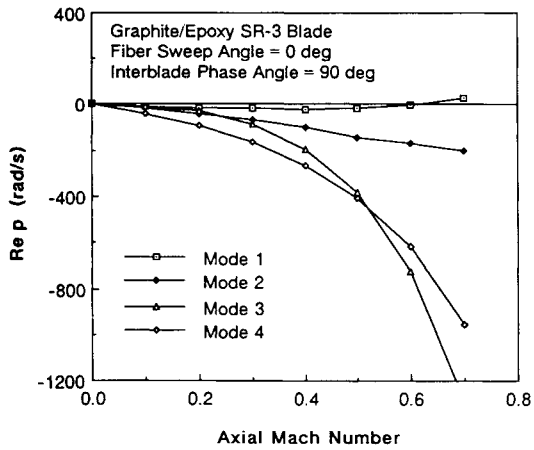

Fig. 7 Modal flutter results for fiber sweep of 0 deg.

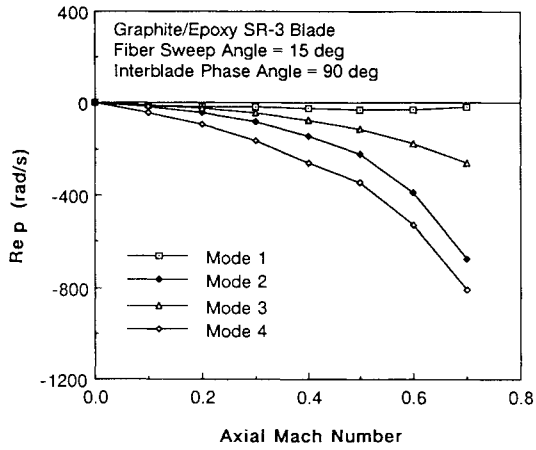

Fig. 8 Modal flutter results for fiber sweep of 15 deg.

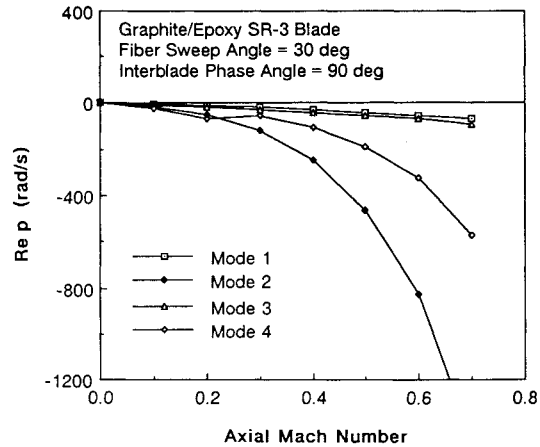

Fig. 9 Modal flutter results for fiber sweep of 30 deg.

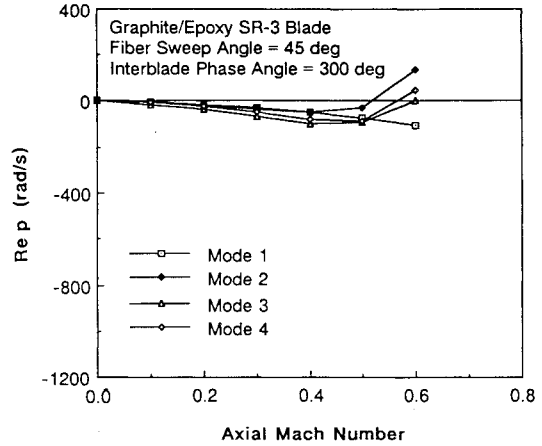

Fig. 10 Modal flutter results for fiber sweep of 45 deg.

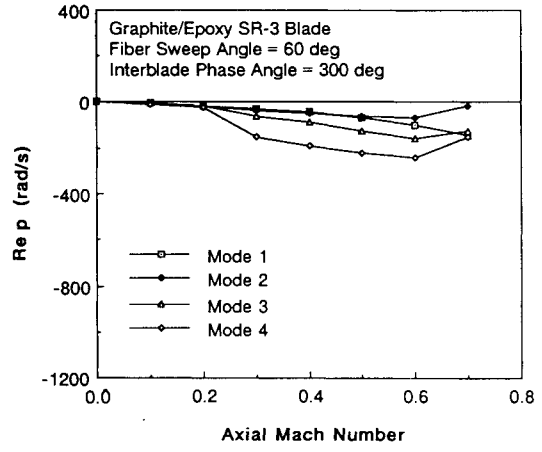

Fig. 11 Modal flutter results for fiber sweep of 60 deg.

Tailoring Effects on Blade Natural Modes and Frequencies

The effects of fiber orientation on the stationary natural frequencies and corresponding modes of the graphite/epoxy SR-3 blade were examined. A 12-element model was used in the analysis. The fiber orientation was assumed uniform over the blade and the section was assumed to have homogeneous anisotropy. Since the section properties vary along the elastic axis, each element was approximated as a straight-line element. The density and the engineering constants along the fiber orientation were taken as follows: 1) density: $\rho_c = 1.6 \times 10^3$ (kg/m^3); 2) elastic moduli: $E_L = 1.4 \times 10^{11}$, $E_T = 1.4 \times 10^{10}$, $G_{LT} = 6.6 \times 10^9$ (N/m^2); and 3) Poisson's ratios: $\nu_{LT} = 0.21$, $\nu_{TT} = 0.21$. The fiber orientation Λ_F is defined to be zero when the orientation coincides with the pitch-change axis and to be positive when swept back, as is shown in Fig. 4a.

The results shown in Fig. 5 indicate that the natural frequencies of graphite/epoxy blade can be controlled by changing the fiber orientation. The first-flap bending frequency, for example, can be changed from its baseline value to 53%. The maximum value of the first-flap bending frequency is obtained when fibers are oriented along the elastic axis, which corresponds to 23 deg in the figure. The corresponding natural modes can also be changed by fiber orientation. This point will be discussed later when the flutter characteristics are described.

Campbell diagram in vacuo (blade natural frequencies vs rotational velocity) is shown in Fig. 6 for the case of the fiber sweep of 30 deg and pitch setting of 60.7 deg. Natural frequencies of flap bending have a tendency to become higher as the rotational velocity increases.

Aeroelastic Tailoring Effects on Flutter Velocity

Throughout the flutter analysis, advance ratio $J = \pi V/\Omega R$ ($=3.0$) and blade-pitch setting $\beta_{0.75}$ ($=60.7$ deg) were kept constant, and flight Mach number M was changed proportionally with the rotor speed Ω, assuming the interblade-phase angle σ as a parameter. The blade material is the same as the previous section. The geometry was the SR-3 model with a diameter of 0.622 m and the number of blades was taken to be eight. Twelve spanwise elements and six modes were used in the modal p-k analysis.

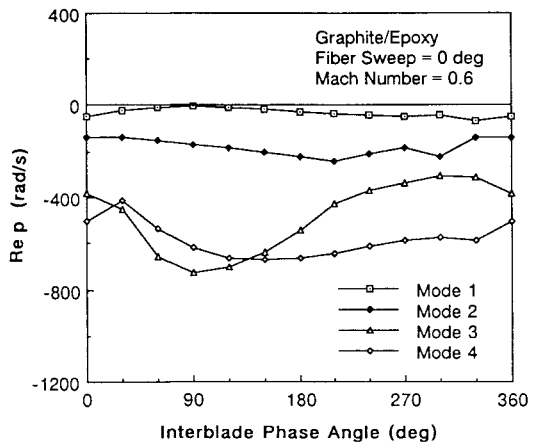

Fig. 12 Effect of interblade-phase angle on modal damping (mode 1 unstable).

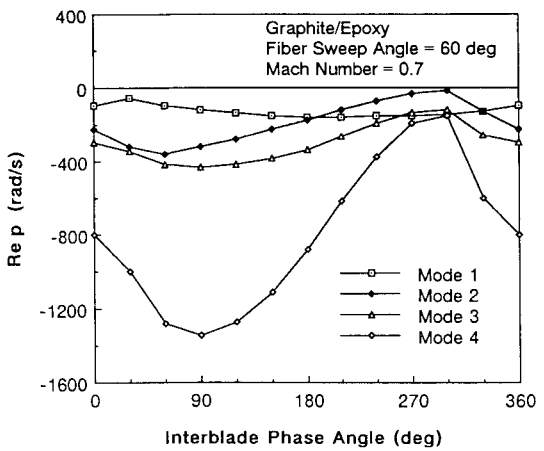

Fig. 13 Effect of interblade-phase angle on modal damping (mode 2 unstable).

By varying the Mach number and the rotational velocity simultaneously, and changing the fiber orientation as a parameter, the p-k flutter analyses were conducted. The fiber orientation is changed from 0 to 60 deg, as shown in Figs. 7–11. Each figure corresponds to the least stable interblade-phase angle for each fiber orientation. Flutter does not occur for a fiber-sweep angle of 30 deg (Fig. 9) when fiber sweep angle is somewhat larger than the elastic axis, since all the real parts of the converged eigenvalues are negative. However, a small change in fiber orientation (e.g., 15 deg), is sufficient to cause flutter. Mode 1, which is the first-flapwise bending mode, has low damping and flutter occurs for the fiber-sweep angles of 15 deg or less (Figs. 7 and 8). Mode 2, which is either the second flapwise bending mode or the first torsion mode (as will be shown later in Fig. 14), becomes unstable for fiber-sweep angles of 45 deg or more (Figs. 10 and 11). This clearly illustrates the sensitivity of the flutter velocity to fiber orientation. The effects of interblade-phase angle can be seen in Figs. 12 and 13, where variation of the real part of eigenvalues is shown. Each figure respectively corresponds to the instability of mode 1 or 2. These plots provide a good illustration of the sensitivity of the eigenvalues to interblade-phase angle.

In order to clarify the characteristics of the natural modes, modes which correspond to stable and unstable conditions are shown in Fig. 14. Only the first four modes are shown, these were selected from the six modes used in the calculation. For the case of zero-fiber sweep, the first-flapwise bending mode which tends to be unstable, has bending-torsion coupling. For the case of the fiber sweep of 60 deg, the first-flapwise bending mode also has bending-torsion coupling but the second mode tends to be unstable. For the case of the fiber sweep of 30 deg, the first-flapwise bending mode and the first-torsion mode have almost no bending-torsion coupling. The mode having no bending-torsion coupling may correspond to the stable condition. This trend is similar to the observations made in Ref. 3.

Concluding Remarks

This article presents a relatively simple aeroelastic analysis tool which is useful for the preliminary design of the ATP blades, and can also be used for trend-type studies aimed at

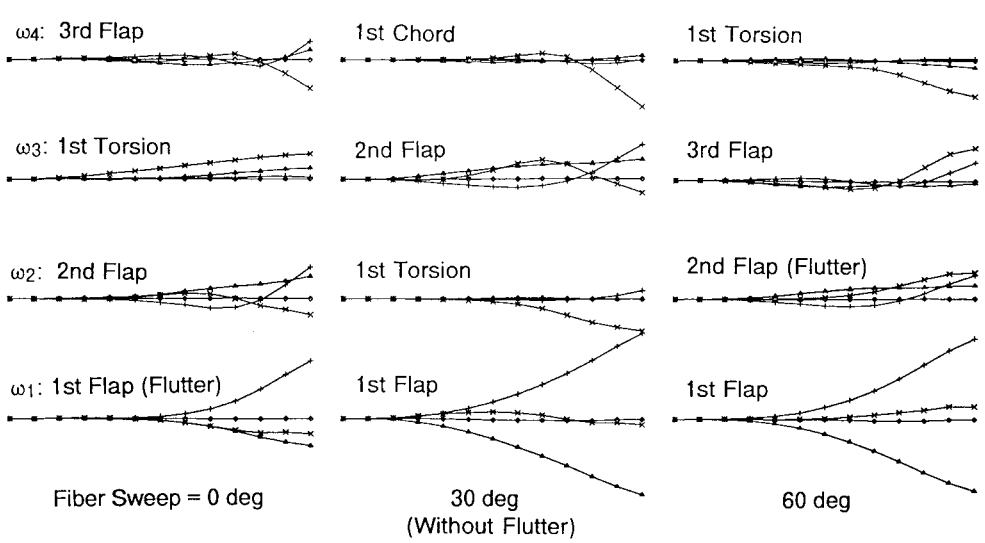

Fig. 14 Effect of natural modes on flutter [fiber sweep = 0, 30, and 60 deg; symbols: Δ = v (lead), + = w (flap), × = ϕ (torsion), ◇ = u (elongation)].

exploring the role of aeroelastic tailoring for suppressing flutter in ATP blades. The structural dynamic model is based on rotating beam finite elements with homogeneous anisotropy, moderate deflections, and section warping which are representative of composite pretwisted blades, and is combined with the unsteady subsonic cascade theory modified for sweep and finite span corrections based on the modified strip theory. Flutter analysis is based on the p-k method after reducing nodal DOFs by a normal mode transformation.

Using this tool, the aeroelastic analysis for the SR-3 propeller model made of graphite/epoxy, was carried out. It was found that the first-bending frequency for the blade can be changed from its baseline value by 53% when changing fiber orientation. It was also shown that fiber orientation which is somewhat larger than the sweep-angle of the elastic axis can eliminate flutter without any weight penalty. Furthermore, it was found that the corresponding first natural mode has the least amount of bending-torsion coupling. However, the flutter velocity was sensitive to fiber orientation and interblade-phase angle.

These results demonstrate the effectiveness of the aeroelastic tailoring in eliminating flutter for advanced turbo propellers. The versatility of this analysis tool for trend and preliminary design-type studies is also clearly illustrated.

Acknowledgments

The authors express their gratitude to John B. Kosmatka, University of California San Diego, AMES Department, for his advice and to Oral Mehmed, NASA Lewis Research Center, for his useful suggestions.

References

[1]Mehmed, O., Kaza, K. R. V., Lubomski, J. F., and Kielb, R. E., "Bending-Torsion Flutter of a Highly Swept Advanced Turboprop," NASA TM 82975, Oct. 1982.

[2]Mehmed, O., and Kaza, K. R. V., "Experimental Classical Flutter Results of a Composite Advanced Turboprop Model," NASA TM 88792, July 1986.

[3]Turnberg, J. E., "Unstalled Flutter Stability Predictions and Comparisons to Test Data for a Composite Propfan Model," NASA CR 179512, Oct. 1986.

[4]Ducharm, E. H., and Crawley, E. F., "Velocity Scaled Aeroelastic Testing of an Unducted Fan," Gas Turbine Lab. Rept. 191, Massachusetts Inst. of Technology, Cambridge, MA, Sept. 1987, pp. 139–231.

[5]Kaza, K. R. V., Mehmed, O., and Williams, M., "Analytical and Experimental Investigation of Mistuning in Propfan Flutter," Structures, Structural Dynamics and Materials Conf., AIAA Paper 87-0739, Monterey, CA, Pt. 2A, April 1987, pp. 98–110.

[6]Elchuri, V., and Smith, G. C. C., "NASTRAN Flutter Analysis of Advanced Turbopropellers," NASA CR-167926, April 1982.

[7]Kaza, K. R. V., Mehmed, O., Narayanan, G. V., and Murthy, D. V., "Analytical Flutter Investigation of a Composite Propfan Model," Structures, Structural Dynamics and Materials Conf., AIAA Paper 87-0738, Monterey, CA, Pt. 2A, April 1987, pp. 84–97.

[8]Kosmatka, J. B., and Friedmann, P. P., "Vibration Analysis of Composite Turbopropellers Using a Nonlinear Beam-Type Finite-Element Approach," *AIAA Journal*, Vol. 27, No. 11, 1989, pp. 1606–1614.

[9]Kosmatka, J. B., "Structural Dynamic Modeling of Advanced Composite Propellers by the Finite Element Method," Ph.D. Dissertation, Mechanical, Aerospace and Nuclear Engineering Dept., Univ. of California, Los Angeles, CA, 1986.

[10]Smith, S. N., "Discrete Frequency Sound Generation in Axial Flow Turbomachines," Aeronautical Research Council R&M 3709, Farnborough, England, UK, March 1972.

[11]Jones, R. M., "Mechanics of Composite Materials," Scripta, Washington, DC, 1975, pp. 31–41.

[12]Kosmatka, J. B., "A Refined Beam Theory for Advanced Composite Rotor Blade Analysis," Specialist Meeting on Advanced Rotorcraft Structures, American Helicopter Society, Rensselaer Polytechnic Inst., Troy, NY, Oct. 1988.

[13]Lekhnitskii, S. G., "Theory of Elasticity of an Anisotropic Elastic Body," Holden-Day, 1963, pp. 191–197, 313–316.

[14]Glauert, H., "Airplane Propellers," *Aerodynamic Theory*, Vol. 4, Dover, New York, 1963, pp. 235–239, 261–269.

[15]Yates, E. C., Jr., "Modified Strip Analysis Method for Predicting Wing Flutter at Subsonic to Hypersonic Speeds," *Journal of Aircraft*, Vol. 3, No. 1, 1966, pp. 25–29.

[16]Bispringhoff, R. L., Ashley, H., and Halfman, R. L., "Aeroelasticity," Addison-Wesley, Reading, MA, 1955, pp. 250–251.

[17]Hassig, H. J., "An Approximate True Damping Solution of the Flutter Equation by Determinant Iteration," *Journal of Aircraft*, Vol. 8, No. 6, 1971, pp. 885–889.

[18]Turnberg, J., "Classical Flutter Stability of Swept Propellers," Structures, Structural Dynamics and Materials Conf., AIAA Paper 83-0847, Lake Tahoe, NV, May 1983.

[19]Rohrbach, C., Metzger, F. B., Black, D. M., and Ladden, R. M., "Evaluation of Wind Tunnel Performance Testing of an Advanced 45° Swept Eight-Bladed Propeller at Mach Numbers from 0.45 to 0.85," NASA CR-3505, April 1982, pp. 52–53, 103–104.